2016

# Development of a Novel *in vivo* Corneal Fibrosis Model in the Dog

K. M. Gronkiewicz
*College of Veterinary Medicine, Columbia*

Elizabeth A. Giuliano
*College of Veterinary Medicine, Columbia*

K. Kuroki
*College of Veterinary Medicine, Columbia*

F. Bunyak
*University of Missouri, Columbia*

Ajay Sharma
*Chapman University*, sharma@chapman.edu

*See next page for additional authors*



## Recommended Citation

Gronkiewicz K, Giuliano E, Kuroki K, et al. Development of a novel *in vivo* corneal fibrosis model in the dog. *Exp Eye Res*. 2016;143:75-88. doi:10.1016/j.exer.2015.09.010.

# Development of a Novel *in vivo* Corneal Fibrosis Model in the Dog




## Authors

K. M. Gronkiewicz, Elizabeth A. Giuliano, K. Kuroki, F. Bunyak, Ajay Sharma, L. B. C. Teixeira, C. W. Hamm, and R. R. Mohan

HHS Public Access

Author manuscript

*Exp Eye Res*. Author manuscript; available in PMC 2017 February 01.

Published in final edited form as:

*Exp Eye Res*. 2016 February ; 143: 75–88. doi:10.1016/j.exer.2015.09.010.

# Development of a novel *in vivo* corneal fibrosis model in the dog

**KM Gronkiewicz**[1,2], **EA Giuliano**[1,2], **K Kuroki**[3], **F Bunyak**[4], **A Sharma**[1,2], **LBC Teixeira**[5], **CW Hamm**[6], and **RR Mohan**[1,2,6,*]

[1]Department of Veterinary Medicine and Surgery, College of Veterinary Medicine, Columbia, Missouri

[2]Harry S. Truman Memorial Veteran Hospital, Columbia, Missouri

[3]Department of Veterinary Pathobiology, College of Veterinary Medicine, Columbia, Missouri

[4]Department of Computer Science, University of Missouri, Columbia, Missouri

[5]Department of Pathological Sciences, School of Veterinary Medicine, University of Wisconsin-Madison, Wisconsin

[6]Mason Eye Institute, University of Missouri, Columbia, Missouri

## Abstract

The aim of this study was to develop a novel in vivo corneal model of fibrosis in dogs utilizing alkali burn and determine the ability of suberanilohydroxamic acid (SAHA) to inhibit corneal fibrosis using this large animal model. To accomplish this, we used seven research Beagle dogs. An axial corneal alkali burn in dogs was created using 1 N NaOH topically. Six dogs were randomly and equally assigned into 2 groups: A) vehicle (DMSO, 2 μL/mL); B) anti-fibrotic treatment (50 μM SAHA). The degree of corneal opacity, ocular health, and anti-fibrotic effects of SAHA were determined utilizing the Fantes grading scale, modified McDonald-Shadduck (mMS) scoring system, optical coherence tomography (OCT), corneal histopathology, immunohistochemistry (IHC), and transmission electron microscopy (TEM). The used alkali burn dose to produce corneal fibrosis was well tolerated as no significant difference in mMS scores between control and treatment groups ($p=0.89$) were detected. The corneas of alkali burned dogs showed significantly greater levels of α-smooth muscle actin, the fibrotic marker, than the controls ($p=0.018$). Total corneal thickness of all dogs post-burn was significantly greater than baseline OCT images irrespective of treatment ($p=0.004$); TEM showed that alkali burned corneas had significantly greater minimum and maximum interfibrillar distances than the controls ($p=0.026$, $p=0.018$). The tested topical corneal alkali burn dose generated significant opacity and fibrosis in dog corneas without damaging the limbus as evidenced by histopathology, IHC, TEM, and OCT findings, and represents a viable large animal corneal fibrosis *in vivo* model. Additional in vivo SAHA dosing studies with larger sample size are warranted.

Corresponding author: Rajiv R. Mohan, Ph.D., FARVO, University of Missouri, 1600 E. Rollins Rd, Columbia, MO 65211, Tel: (573) 884-1449, Fax: (573) 884-4100, mohanr@health.missouri.edu.

## Graphical abstract

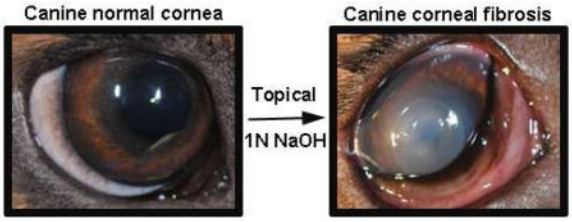


### Keywords

Alkali burn; dog; α-smooth muscle actin; corneal fibrosis; suberanilohydroxamic acid

## 1. Introduction

Ocular injury threatens short and long-term corneal clarity and vision. Both human and veterinary patients are commonly subject to corneal injury, the cause of which may be pathologic (e.g. trauma, infection, other) or surgical (e.g. status post corneal transplant or photorefractive keratectomy (PRK), conjunctival grafting procedures, other (Pumphrey et al. 2011, Gray and West 2014, Labelle et al. 2014, Guell et al. 2015). Regardless of the exact etiology the resulting sequela is often loss of corneal transparency due to dysregulated healing and subsequent fibrosis (Fini and Stramer 2005). Corneal fibrosis can result in blindness, rendering a person unable to read, write, operate a vehicle and perform other required daily tasks. Similarly, corneal fibrosis is debilitating to veterinary patients. The loss of corneal transparency impairs the animal's visual field and depth perception resulting in decreased performance as visually impaired German Shepherd dog is unable to execute search and rescue operations, a Golden Retriever working as a guide dog for the blind patients cannot assist its owner, and a racing horse cannot compete in flat races, polo sports, or display jumping. The inability of service animal to perform result in an animal's immediate, premature retirement and potentially even euthanasia especially when the blind animal is a danger to people. The loss of service animals suffering from corneal fibrosis is emotional to trainers and owners and financially devastating for government and not-for-profit organizations. Corneal fibrosis remains one of the leading causes of blindness in animals and people worldwide (Pascolini and Mariotti 2012, Robaei and Watson 2014). Thus, the development of novel, successful strategies to treat corneal fibrosis remains an important goal for both physician and veterinary ophthalmologists.

Both *in vitro* and *in vivo* study designs have been used to investigate different treatment strategies that may prevent corneal fibrosis. Research performed in an *in vitro* setting utilizes cell culture (Pan et al. 2009, Nelson et al. 2012). Cell culture lacks the different inflammatory cells, growth factors, and cytokines that are key players in corneal wound healing, and therefore, ultimately fail to replicate the complicated process of wound healing *in vivo*. Small laboratory animal species such as rodents and rabbits are commonly used in current corneal fibrosis research (Milani et al. 2013, Gu et al. 2014). While the *in vivo* studies overcome the limitations of *in vitro* experiments by representing native corneal wound healing, the cornea of rats, rabbits and mice differ significantly from those of people

in terms of thickness and diameter (Vezina 2013). An animal model possessing corneal anatomy and physiology similar to people is important for determining bench-to-bedside translational potential of anti-fibrotic treatments to clinical application in human and veterinary clinics. The dog represents an ideal animal model for studying molecular mechanisms mediating corneal fibrosis and testing the efficacy and safety of therapies for corneal scarring and restoring vision. Not only are the dog's corneal dimensions comparable to people (Vezina 2013), they are common veterinary patients presenting with ocular injuries similar to humans that result in corneal fibrosis (Kern 1990). Thus, developing a model of corneal fibrosis and discovering a successful anti-fibrotic agent in dogs would impact both physician and veterinary ophthalmology.

Eye trauma, injury and infection result in changes within the corneal stroma, as the previously quiescent keratocytes are activated to repair the cornea. During corneal wound repair, keratocytes undergo migration, proliferation, apoptosis, extracellular matrix remodeling, and cellular trandifferentiation, generating myofibroblasts. Several growth factors, cytokines, and chemokines regulate these processes and dysregulation of these repair mechanisms can result in corneal fibrosis (Sharma et al. 2009 and Tandon et al. 2012, Stramer et al 2003, Hassell and Birk 2010). Of the various factors implicated in the formation of the corneal fibrosis, transforming growth factor (TGF-β) plays a significant role, facilitating the conversion of keratocytes to myofibroblasts through modulation of Smad proteins, matrix metalloproteinases, and transcriptional activity, specifically histone deacetylation (Sharma et al 2015). It has been established that TGF-β-induced overexpression of histone deacetylases (HDAC) contributes to the development of corneal fibrosis (Guo et al. 2009, Zhou et al. 2010). Consequently the inhibition of these enzymes represents a means by which pro-fibrotic intracellular signaling can be blocked. The therapeutic potential of histone deacetylase inhibitors (HDACi) as anti-fibrotic agents has demonstrated extreme promise in different models of corneal fibrosis. For instance, trichostatin A, an inhibitor of class I and II HDACs, was shown to effectively decrease corneal fibrosis in rabbits *in vivo* following photorefractive keratectomy surgery (Sharma et al. 2009). Another HDACi, suberanilohydroxamic acid (SAHA) which is FDA approved, tested in our laboratory demonstrated significant inhibition of TGF-β1-mediated fibrosis in canine and equine cornea *in vitro* and rabbit cornea *in vivo* (Bosiack et al. 2012, Tandon et al. 2012, Donnelly et al. 2014). A recent study from our laboratory found that anti-fibrotic effects of SAHA are partially mediated by the transcriptional repressors 5′TG3′-interacting factors (TGIF) 1 and TGIF2 in human cornea *in vitro* (Sharma et al. 2015). The clinical use of SAHA as an anti-fibrotic agent in human patients demands translational research utilizing a large *in vivo* animal model that has a cornea comparable to that of the human cornea.

Current *in vivo* models of corneal fibrosis used to investigate anti-fibrotic agents utilize various methodologies such as sulfur mustard exposure, laceration and suture, and alkali burn (Berdahl et al. 2009, Kadar et al. 2013, Okada et al. 2014). The alkali burn is easy to perform, does not require specialized equipment and presents minimal risk to those performing the procedure. It also results in significant fibrosis and neovascularization. To our knowledge, the current literature lacks a study describing the use of the alkali burn to create corneal fibrosis in dogs. Therefore, it was the purpose of this study to develop and

describe a novel *in vivo* model of corneal fibrosis in dogs using the alkali burn. Additionally, the efficacy of the experimental anti-fibrotic agent SAHA was investigated in the current study. It was hypothesized that the alkali burn would create significant fibrotic changes in the canine cornea and that SAHA would prevent fibrosis in these wounded dog corneas.

## 2. Methods

### 2.1. Animals

Seven healthy female Beagle dogs (9–12 months, 10–15 kg) were purchased from Covance Laboratory (Cumberland, VA) and housed in a research facility at the University of Missouri. Prior to the onset of the study all dogs underwent a complete ophthalmic examination by a board certified veterinary ophthalmologist (EAG) which included slit lamp biomicroscopy (SL-15 Kowa Company, Ltd, Tokyo, Japan), indirect ophthalmoscopy (Wireless indirect ophthalmoscope, Keeler Instruments Inc., Broomall, PA, USA and pan retinal 2.2 indirect lens, Volk Optical Inc., Mentor, OH, USA), Schirmer tear test I (Schering-Plough Animal Health, Union, NJ, USA), tonometry (Tono-Pen Vet, Dan Scott and Associates, Westerville, OH, USA) and fluorescein staining (Flu-Glo, Akorn, Inc., Buffalo Grove, IL, USA). All dogs were determined to be free of ocular disease. The dogs received daily socialization and all other husbandry needs including a diurnal 12 hour light cycle. All studies were performed in accordance with the ARVO Statement for the Use of Animals in Ophthalmic and Vision Research and were approved by the University of Missouri Institutional Animal Care and Use Committee.

### 2.2. Baseline Anterior Segment Optical Coherence Tomography (OCT)

Imaging was performed with a Heidelberg Spectralis® OCT (Heidelberg Engineering, Heidelberg, Germany) which was equipped with an Anterior Segment Module attachment to shift the focal plane from the retina to the cornea. The Heidelberg system functions at 815 nm and can perform 40,000 A-scans per second. The imaging unit has a working distance of 11–14 mm, depending on the axial length of the eye and the type of pathology being imaged.

To obtain baseline OCT images, animals were sedated with dexmedetomidine (Zoetis Inc., Kalamazoo, MI, USA, 7 mcg/kg, IM). They were then placed and maintained in sternal recumbancy with gentle manual restraint. A 6 mm corneal pachymetry protocol was performed by a single operator (CWH). After bringing the objective lens close to the cornea, the image was aligned to the axial cornea, and only scans that were free of motion artifact were accepted for data analysis. Upon completion of OCT imaging, atipamazole hydrochloride (Zoetis Inc., Kalamazoo, MI, USA, volume equivalent to that of dexmedetomidine, IM) was administered to reverse the effects of dexmedetomidine.

Image analysis of normal corneas included measurements of both epithelial and total corneal thickness. For each image, single measurements of these parameters were made using the measurement calipers provided by the AS-OCT software.

### 2.3. Development of Corneal Alkali Burn in a Sentinel Dog

To effectively develop the novel model of canine corneal fibrosis *in vivo*, a sentinel dog underwent focal corneal alkali burn of each eye at separate time points. The corneal wounding was performed by a board certified veterinary ophthalmologist (EAG). The animal was sedated with dexmedetomidine (7mcg/kg, IM) and hydromorphone (0.1 mg/kg, IM). Following sterile placement of an intravenous catheter, propofol (Abbott Animal Health, Abbott Park, IL, USA, 2–4 mg/kg, IV) was administered until the animal was at an appropriate level of anesthesia for intubation. However, intubation was only considered necessary if apnea occurred, and anesthesia was maintained with IV administration of propofol to effect. The right eye was then aseptically prepared, using a 1:20 dilution of betadine solution, and then local anesthetic medication (proparacaine hydrochloride 1%, Bausch & Lomb Inc., Tampa, FL, USA) was applied to this eye 3 times to numb the corneal surface. Topical mydriatic and cycloplegic agent (atropine sulfate 1%, Bausch & Lomb Inc., Tampa, FL, USA) was then applied once.

To perform the alkali burn, a 6 mm diameter filter paper disc was soaked in 1 N NaOH. The disc was then promptly applied to the axial cornea of the right eye for 15 seconds. Following removal of the filter paper disc the cornea was rinsed with sterile phosphate buffered saline for 60 seconds. After the cornea was thoroughly rinsed, fluorescein stain was applied topically to verify the corneal burn and resulting ulceration. Atipamazole hydrochloride (volume equivalent to that of dexmedetomidine, IM) was administered to reverse the effects of dexmedetomidine and the dog was then routinely recovered from the short anesthetic episode.

The dog received standard treatment for corneal ulceration including topical antibiotic (Bactracin, polymyxin B, gramicidin ophthalmic solution, Paddock Laboratories Inc., Minneapolis, MN, USA 1 drop OD q 8 hr), topical mydriatic and cycloplegic (atropine sulfate 1.0%, ophthalmic solution, Akorn Inc., Lake Forest, IL, USA, 1 drop to effect), systemic anti-inflammatory medication (carprofen, Zoetis Inc., Kalamazoo, MI, USA, 2.2 mg/kg PO q 12 hr) and systemic analgesic medication (tramadol, Amneal Pharmaceuticals, Bridgewater, NJ, USA, 4 mg/kg, PO q 12 hr). To prevent ocular self-trauma the dog also wore an Elizabethan collar until the study's endpoint.

Daily examinations and minimally invasive ophthalmic diagnostic testing (fluorescein stain application) were performed for 14 days. Using slit-lamp biomicroscopy, ocular health was graded according to the modified McDonald-Shadduck (mMS) scoring system. Corneal haze was assigned a numerical grade according to the Fantes grading scale (range from 0–4). Photography of the right eye was performed daily both prior to and after fluorescein stain application, using a Nikon D300S camera and AF-S DX NIKKOR 18–200mm f/3.5–5.6G ED VR II lens (Nikon Inc., Melville, NY, USA).

Once the corneal ulcer of the right eye had completely healed, the left eye underwent an alkali burn. The dog was anesthetized and the eye was surgically prepared as previously described. A 6 mm diameter filter paper disc soaked in 1 N NaOH was applied to the axial cornea of the left eye for 30 seconds and the cornea was then immediately flushed with phosphate buffered saline for 60 seconds. Fluorescein stain was topically applied confirming

the presence of an ulcer. The dog then underwent identical treatment, examination, diagnostic testing and imaging as previously described for 14 days. At this end point, OCT imaging was repeated as previously described. Due to the variable thickness of the corneal epithelium following the alkali-burned, four different areas of the epithelium were measured in each image and values were averaged. A single measurement of total axial corneal thickness was obtained. Any abnormal lesions were noted and described with regards to their size and degree of reflectivity. The dog was then humanely euthanized with pentobarbital (100 mg/kg, IV) under sedation. Corneas were excised and samples were stored in appropriate media for histopathology, IHC, and TEM respectively.

### 2.4. Preparation of Vehicle and SAHA

Topical SAHA or vehicle were administered to the 6 additional study dogs following the corneal alkali burn. These topical agents were prepared by an individual masked to the study design. To prepare topical vehicle, 10 μL of dimethylsulfoxide (DMSO, Sigma-Aldrich Corp., St. Louis, MO, USA) was added to 2 mL of phosphate buffered saline in a sterile eye dropper bottle, labeled “A”, to achieve a final concentration of 2 μL/mL. For the preparation of topical SAHA, a 10 mM stock solution of SAHA (Caymam Chemical Company, Ann Arbor, MI, USA) was made by dissolving 1.3 grams of SAHA in 500μL of dimethylsulfoxide (DMSO). Then, to achieve a final concentration of 50 μM, 10 μL of the 10 mM stock solution of SAHA was added to 2 mL of phosphate buffered saline in a sterile eye dropper bottle, and labeled “B”.

### 2.5. Corneal Alkali Burn in 6 Additional Dogs

Prior to performing the alkali burn, 6 dogs were randomly assigned to one of 2 treatment groups (3 dogs/group). Group A served as control, receiving topical vehicle in addition to the previously described standard treatment for corneal ulceration. Group B, the experimental group, received topical SAHA (50 μM) and standard treatment for corneal ulceration.

Corneal wounding was performed by a board certified veterinary ophthalmologist (EAG). To perform the alkali burn, the dogs were anesthetized, and the right eye was surgically prepared as previously described for the sentinel dog. Based on the results of the sentinel dog’s alkali burn of 15 and 30 seconds respectively, a 6 mm diameter filter paper disc soaked in 1 N NaOH was applied to the axial cornea of the right eye for 20 seconds. After the affected cornea was rinsed with phosphate buffered saline for 60 seconds fluorescein stain was topically applied. The dogs then received the standard of care for corneal ulceration and topical vehicle (Group A) or SAHA (Group B). Both vehicle and SAHA were administered q 8 hr. Elizabethan collars were worn by all dogs.

The dogs underwent daily examinations by a veterinary ophthalmologist (EAG) masked to treatment group and were scored using the mMS and Fantes grading systems. Diagnostic testing and imaging as previously described for the initial dog was performed at each examination until the study’s endpoint (day 14). At study endpoint OCT imaging was repeated as previously described: four different areas of epithelium and a single total axial corneal thickness measurements were taken and any abnormal lesions were described with

regards to their size and degree of reflectivity. Dogs were humanely euthanized with pentobarbital (100 mg/kg, IV) under sedation, and corneas were excised, subsectioned, and stored appropriately for histopathology, IHC and TEM. Normal corneas from 3 dogs of different breeds (Miniature Poodle, American Pit bull terrier and mixed breed dog) that were being euthanized for reasons unrelated to the study were used as negative controls for histopathology, IHC, and TEM.

### 2.6. Histopathological Analysis of H&E, Masson's Trichrome, Elastica van Gieson and Periodic acid-Schiff Stained Corneal Sections

Corneas were halved using sharp dissection with one section being placed in 10% buffered formalin for histopathological analysis and the other stored for TEM (see TEM methodology). After routine histologic processing, 5 μm sections were mounted on glass slides for staining with hematoxylin and eosin (H&E), Masson's trichrome, picrosirius red, elastica-van Gieson (EVG) and periodic acid-Schiff (PAS). H&E, Masson's trichrome, EVG and PAS stained slides were examined using light microscopy by a masked, board-certified veterinary pathologist (KK). Picrosirius red slides were evaluated by a masked, board-certified veterinary pathologist (LBCT) (see next section). Corneal tissue sections were described and evaluated for any histopathological abnormalities, specifically neovascularization and edema. The severity of the neovascularization and edema on H&E and staining intensity in the anterior stroma of the Masson's trichrome, EVG and PAS stained corneas were subjectively assigned a grade from 0–3. The component of stain scored and grading scale are described in Tables 1 and 2 respectively.

### 2.7. Histopathological Analysis of Picrosirius Red Stained Corneal Sections

The picrosirius red stained slides were analyzed using a bright field microscope (Olympus BX43, Melville, NY). Images were captured by a mounted digital camera (Olympus DP72, Melville, NY) and analyzed using an image analysis software (CellSence Dimension 1.6, Olympus, Melville, NY). The collagen type composition of the corneal stroma was measured using picrosirius red stained sections under polarized light following previously published protocols.(Junqueira, Cossermelli et al. 1978, Whittaker 2005) Briefly, the superficial corneal stroma of the treated areas was photographed under 400X magnification and using image analysis software the total collagen area and proportion of red-yellow-orange fibers (type I collagen) and green fibers (type III collagen) were quantified.

### 2.8. Immunohistochemistry

Unstained, paraffin embedded tissue sections (5 μm) underwent immunohistochemical staining to further characterize the pathologic changes subsequent to the alkali burn by one author (KK). Antibodies used included α-smooth muscle actin (α-SMA) which is a hallmark of fibrosis (Dako, #M0851, diluted 1:300) and CD18 which is expressed by all leukocytes (UC-Davis, #CA16.3C10, diluted 1:80). Staining intensity was assigned a grade from 0–3, with 0 representing no staining, 1–3 representing mild, moderate, marked staining, respectively.

### 2.9. TEM Sample Preparation and Image Capture

All reagents for this study's TEM were purchased from Electron Microscopy Sciences and all specimen preparation was performed at the Electron Microscopy Core, University of Missouri, Columbia, MO, USA. Tissues were fixed in 2% paraformaldehyde, 2% glutaraldehyde in 100 mM sodium cacodylate buffer pH=7.35. Next, fixed tissues were rinsed with 100 mM sodium cacodylate buffer, pH 7.35 containing 10 mM 2-mercaptoethanol (Sigma Aldrich, St. Louis, MO, USA) and 130 mM sucrose (further referred to as 2-ME buffer). Secondary fixation was performed using 1 % osmium tetroxide (Ted Pella, Inc. Redding, California, USA) in 2-ME buffer using a Pelco Biowave (Ted Pella, Inc. Redding, California, USA) operated at 100 Watts for 1 minute. Specimens were next incubated at 4 °C for 1 hour and then rinsed with 2-ME buffer, which was followed by distilled water. Using the Pelco Biowave, a graded dehydration series (per exchange, 100 Watts for 40 s) was performed using ethanol, transitioned into acetone, and dehydrated tissues were then infiltrated with Epon/Spurr's resin (250 Watt for 3 min) and polymerized at 60 °C overnight. Sections were cut to a thickness of 85 nm using an ultramicrotome (Ultracut UCT, Leica Microsystems, Germany) and a diamond knife (Diatome, Hatfield, PA, USA). These sections were post-stained using Sato's triple lead solution stain(Sato 1968) and 5% aqueous uranyl acetate. Images were acquired with a JEOL JEM 1400 transmission electron microscope (JEOL, Peabody, MA, USA) at 80 kV on a Gatan Ultrascan 1000 CCD (Gatan, Inc, Pleasanton, CA, USA). For each cornea, four images were acquired from different areas of the anterior stroma at a magnification of 25,0000X with collagen fibrils cut in cross section for subsequent analysis.

### 2.10. TEM Image Analysis and Quantification

For automated quantification of corneal collagen fibrils in TEM images, an in-house image processing and analysis software was developed. This image analysis pipeline consisted of three main modules, (i) fibril detection, (ii) shape analysis and cluster decomposition, and (iii) size and interfibrillar distance analysis.

Multi-scale Hessian matrix was used to detect collagen fibrils. Hessian matrix (Equation 1) described the second order structure of local intensity variations around each point of the image L(x,y), and eigenvalues $\lambda_{1,2}$ (Equation 2) of Hessian matrix was used to detect blob-like, or ridge-like structures. Table 3 shows possible local orientation patterns based on the eigenvalues of the Hessian matrix.

$$\mathbf{Hessian}_{\sigma}(x,y)=\begin{bmatrix} L_{xx}(x,y) & L_{xy}(x,y) \\ L_{xy}(x,y) & L_{yy}(x,y) \end{bmatrix} \quad (1)$$

$$\lambda_{1,2}=\frac{1}{2}(L_{xx}+L_{yy} \pm \sqrt{(L_{xx}-L_{yy})^2+(2L_{xy})^2}) \quad (2)$$

Hessian matrix was computed by convolving the image with derivatives of the Gaussian kernel, where scale σ represented the standard deviation of the Gaussian kernel and

controlled the radius of the detected structures. A coarse fibril mask was produced by computing Hessian matrix and thresholding $\lambda_1$(Hessian) as below:

$$Mask_{Fibril}(x,y)=\begin{cases} 1 & \lambda_1(\mathbf{Hessian}(x,y))<\varepsilon \\ 0 & \text{otherwise} \end{cases}$$

Quantification of morphology and spatial organization of fibrils required accurate identification and localization of individual fibrils. Hessian-based detection efficiently segmented regions occupied by fibrils from the background but failed to separate some of the neighboring fibrils and merged them into clusters. To identify individual fibrils a shape analysis and cluster decomposition module is developed as based on previously reported modules.(Ersoy, Bunyak et al. 2012, Sun, Huang et al. 2014) Specifically, first connected component labeling was applied to the detection mask and disconnected blobs were identified. Then, to each detected blob $B_i$, an ellipse $E_i$ was fitted. Blob and ellipse areas *area($B_i$)*, *area($E_i$)*, and ratio *r=(area($E_i$)-area($B_i$))/area($B_i$)* were then computed. Using these size and shape indices, and their means and variances over the image, each detected blob $B_i$ was classified into one of the three classes (spurious detection, single fibril, or fibril cluster). Blobs classified as spurious detection were removed; blobs classified as single fibril were kept intact. Marker-controlled watershed transformation was used to decompose fibril clusters into individual fibrils.(Vincent and Soille 1991) Regional maxima of distance transform were used as markers. To suppress spurious regional maxima and to prevent over-segmentation, H-maxima transform was applied to the distance transform prior to the detection of regional maxima.(Soille 1999)

The module then computed parameters related to fibril morphology and spacing, such as fibril radius, fibril area fraction, and interfibrillar distance. From the refined segmentation (Figure 1B), fibril centroids were computed. Delaunay triangulation & vertex coloring were applied to the located centroids, and a colored neighborhood graph was generated, as previously described.(Nath, Palaniappan et al. 2006, Ersoy, Bunyak et al. 2012) In the neighborhood graph (Figure 1C), nodes corresponded to individual fibrils, and edges linked immediate neighbors. For each node in this neighborhood graph, two specific neighbors were identified, specifically the nearest immediate neighbor (Figure 1D red edges) and farthest immediate neighbor (Figure 1D blue edges). A second graph (nearest/farthest neighborhood graph) was constructed, using only these specific links. Fibril-to-fibril interactions were assessed, and spatial organization of collagen fibrils were described using these two neighborhood graphs. Various descriptors from these graphs such as mean and standard-deviation were then calculated.

### 2.11. Statistical Analysis

Statistical analysis was performed by a biostatistician (RWM). The results of the initial corneal wounds in the pilot dog and the corneal haze scores of all dogs are summarized using descriptive statistics. Clinical scoring, OCT measurements, histopathology scores, picrosirius red measurements and TEM measurements from the other study dogs were analyzed statistically. The mMS scores were analyzed with a two factor ANOVA with treatment being a between-subjects factor and time (day) being a within-subjects (or

repeated measures) factor. When evaluating histopathological, immunohistochemistry scores, and picrosirius red measurements between negative controls and alkali-burned corneas, without regards to treatment group, and also between treatment groups, a Wilcoxon rank sum test was utilized. Any difference in the epithelial thickness and total corneal thickness measured in the OCT images between the treatment groups at baseline was detected with a two-sample t-test, while the difference in these measurements between the baseline images and those of alkali-burned corneas was analyzed with a one-sample paired t-test. TEM results were analyzed with a weighted t-test. Weights were used to account for different subsample sizes for the different dogs. All statistical analyses were performed using standard statistical software SAS v9 (SAS Institute Inc., Cary, NC, USA). All p-values $<0.05$ were considered statistically significant.

## 3. Results

### 3.1. Baseline OCT of Normal Corneas

Prior to performing corneal alkali burn, OCT was performed of both eyes of all dogs to obtain particular measurements. In each OCT image of normal cornea three distinct layers of varying thickness and reflectivity were noted which included (i) the pre-corneal tear film and epithelium, (ii) the stroma and (iii) Descemet's membrane and endothelium. However, for the purposes of this study, only the epithelium and anterior stroma were qualitatively described. The corneal epithelium was poorly reflective and located between the highly reflective pre-corneal tear film and the corneal stroma which demonstrated intermediate reflectivity. The reflectivity of both the epithelium and anterior stroma was primarily homogenous, in part due to the fact that dogs do not have a Bowman's membrane.

The mean epithelial thickness of the right eye and left eye was $77.429 \pm 2.878$ μm and $78.571 \pm 3.599$ μm, respectively. There was no statistically significant difference in epithelial thickness of the right eyes between treatment groups at baseline ($p=0.82$). The mean total corneal thickness of the right eye and left eye was $545.714 \pm 42.074$ μm and $555.571 \pm 26.937$ μm, respectively, and there was no statistically significant difference in total corneal thickness of the right eye between treatment groups at baseline ($p= 0.33$).

### 3.2. Corneal Alkali Burn in the Sentinel Dog Supports Development of Fibrosis

The initial mMS scores recorded from the sentinel dog the first day (i.e. day 1) following the alkali burn were 9.5 for the right eye and 10 for the left eye. Ocular health continued to improve throughout the study. Fourteen days after each respective alkali burn, the clinical score of the right eye was 2, which was due to some loss of corneal transparency which occupied 1–25% of the cornea and the clinical score of the left eye was 5.5, which was due to moderate loss of corneal transparency affecting 1–25% of the cornea, mild conjunctival congestion, and a superficial axial corneal ulcer. The corneal haze grade at 14 days post alkali burn was 1 for the right eye and 2 for the left eye.

At the study's endpoint, which was 5 weeks post alkali burn for the right eye and 2 weeks post alkali burn for the left eye, the epithelial thickness of both eyes was variable and the average of four different measurements was $116.75 \pm 28.076$ μm in the right eye while that of the left eye was $114.25 \pm 22.187$ μm. Total corneal thickness of the right eye was 499 μm.

The left eye's total corneal thickness had increased to 973 μm. The changes in epithelial thickness and total corneal thickness are highlighted in Table 4. In the anterior corneal stroma of both eyes, an area of increased reflectivity were noted. The foci extended to a depth of 317 μm in the right eye and 302 μm in the left eye. Additionally, OCT images of the left eye revealed subepithelial foci which were non-reflective, suggestive of corneal edema or bulla formation.

Histopathology of the cornea of the right eye revealed a mildly increased number of stromal nucleated cells in superficial stroma and very small number of inflammatory cells, suggestive of only mild superficial fibrosis. No corneal neovascularization or edema was noted. The scores assigned to the different stains were as followed: Masson's trichrome; 1, EVG: 0, and PAS; 1. Analysis of picrosirius red stain revealed a total collagen area in the wound bed of 34,533 $\mu m^2$. The total area of type I collagen in the wound bed was 31,895 $\mu m^2$ (49% of the area corneal tissue measured). The total area of type III collagen in the wound bed was 2,638 $\mu m^2$ (4.1% of the area corneal tissue measured). IHC demonstrated mild staining for α-SMA and no staining for CD18.

Histopathological analysis of the left eye's cornea revealed corneal epithelial hyperplasia and fibrosis extending to mid-stroma. Mild corneal neovascularization and marked corneal edema were also noted. The scores assigned to the different stains were as follows: Masson's trichrome; 2, EVG: 2, and PAS: 2. Analysis of picrosirius red stain revealed a total collagen area in the wound bed of 38,663 $\mu m^2$. The total area of type I collagen in the wound bed was 37,430 $\mu m^2$ (57% of the area corneal tissue measured). The total area of type III collagen in the wound bed was 1,233 $\mu m^2$ (1.9% of the area corneal tissue measured). The section also demonstrated marked staining for α-SMA and no staining for CD18.

Analysis of the TEM images of the burned corneas revealed that the mean area of the collagen fibrils of the right eye was 846.960 ± 0.0001 $nm^2$, while that of the left eye was 990.818 ± 0.0001 $nm^2$. The mean minimum distance between neighboring collagen fibrils in the right and left eyes was 43.772 ± 0.000005 nm and 46.178 ± 0.000003 nm respectively. The mean maximum distance between neighboring collagen fibrils was 71.348 ± 0.000006 nm for the right eye and 72.5 ± 4.264 nm for the left eye. The representative TEM images of the dog corneas are shown in Figure 1.

### 3.3. Alkali Burn is Well Tolerated and Results in Corneal Opacity in 6 additional dogs: Clinical and Haze Scores

The mMS scores of the dogs were not statistically different between treatment groups at any time point (p=0.89), with the highest score (17.5) being recorded for one dog in each treatment group on day 1 (Figure 2A). The mMS scores continued to decrease until the study's endpoint, with an 8 being recorded as the highest score on day 14, while the majority of dogs received a score of 6.5 (Figure 2D). The progression in clinical scores of a representative dog is shown in Figure 2. The exception was a single dog in group A. Over a period of 24 hours, the corneal wound of this dog acutely worsened and was noted to be malacic on day 11 (Figure 2C). Samples of the cornea were aseptically collected for cytology and culture and sensitivity. The cytology revealed suppurative inflammation with

mild epithelial cell atypia. No infectious organisms were appreciated on cytology. Microbes were not detected with culture. All scores from day 11 to day 14 and OCT, histopathological and TEM findings for this particular dog were excluded from analysis.

Significant corneal opacity secondary to alkali burn was appreciated in all dogs at every time point. At the study's endpoint, the mean corneal haze grade was 1.8 ± 0.447. The formation of corneal haze is demonstrated in Figure 2D.

### 3.4. OCT Findings Support Development of Corneal Fibrosis

The OCT images at the study's endpoint demonstrated several pathologic changes all dogs' right corneas. The reflectivity of the epithelium had increased and the thickness was variable. Images revealed foci of a hyper-intense signal in the anterior stroma. Additionally, some images contained foci within the epithelium that were non-reflective, suggestive of bulla formation. These changes were confined to the axial cornea and did not differ between treatment groups.

Following the alkali burn, the mean epithelial thickness of the six dogs' right eyes was 83.9 ± 23.213 μm, and the mean total corneal thickness was 906.8 ± 148.417 μm. The mean epithelial thickness following the alkali burn did not differ significantly from the baseline epithelial thickness, irrespective of treatment ($p=0.5334$), indicating that alkali-burned corneas re-epithelized, typical of normal corneal wound healing. The mean epithelial thickness of group A was 86.75 ± 20.860 μm, while that of group B was 82.0 ± 25.158 μm. The mean total corneal thickness of all dogs, regardless of treatment group, was statistically greater than that of the baseline images ($p=0.004$). The mean total corneal thickness of group A was 793.50 ± 212.839 μm, while that of group B was 982.333 ± 3.215 μm. The measurements for individual dogs are provided in Table 4. There was no statistical difference between treatment groups regarding epithelial thickness or total corneal thickness ($p=0.837$, $p=0.302$, respectively). These changes detected with OCT are highlighted in Figure 3 as representative OCT images of alkali-burned corneas (Figure 3B and 3C) demonstrated notable increased epithelial and total corneal thickness compared to normal cornea at baseline (Figure 3A).

### 3.5. Fibrotic Changes Appreciated on Histopathology

Various histopathological corneal changes were noted on H&E slides of the alkali-burned corneas and included: mild corneal epithelial hyperplasia, presence of fibrin, a few lymphocytes and neutrophils and many fibrocytic cells in stroma, mild erosion of epithelium and focal absence, thickening, disorganization and destruction of epithelial basement membrane (Figure 4E). Varying degrees of edema and neovascularization formation were noted in all alkali-burned corneas, except for one dog receiving Treatment A who did not appear to develop corneal neovascularization. There was no significant difference between alkali-burned corneas and negative controls when comparing severity of corneal neovascularization or edema ($p=0.107$), and a significant difference in corneal neovascularization or edema formation was not detected between treatment groups ($p=0.3$). The grades for corneal edema and neovascularization are shown in Table 5.

It was grossly apparent that the staining pattern for Masson's trichrome, EVG and PAS stains differed between the negative control and alkali-burned corneas and scores for each stain are displayed in Table 5. The epithelium and anterior stroma of the negative control corneas stained in a homogenously. The epithelium following Masson's trichrome staining appeared red while the stromal collagen fibers stained blue (Figure 4B). Following EVG staining, the epithelium was a dark purple-black color while the stroma stained fuchsia (Figure 4C). Finally, the PAS stained negative control corneas included a light purple epithelium and light pink stroma (Figure 4D). Following the alkali burn, an increased number of spindle fibrocytic cells were noted in the anterior stroma of the Masson's trichrome stained corneas as evidenced by the increased red stain in this area (Figure 4F). The EVG stained alkali-burned corneas showed increased dark purple-black staining in the anterior stoma, suggestive of elastic fiber deposition (Figure 4G). Finally, PAS stained alkali-burned corneas had an increase in dark pink-purple staining in the anterior stroma, suggestive of increased fibrin deposits and/or increased basement membrane formation (Figure 4H). Despite these visually obvious differences between negative control and alkali-burned corneas, no significant difference was detected in this small sample size (Masson's trichrome, $p=0.125$, EVG, $p=0.143$; PAS, $p=0.143$). Similarly, there was no significant difference between treatment groups with regards to the degree of staining (Masson's trichrome, $p=0.6$; EVG, $p=0.4$; PAS, $p=0.5$).

There was a marked, visible contrast between negative control and alkali-burned corneas with picrosirius red staining, as shown in Figure 5. Negative control corneas were primarily comprised of red-yellow-orange fibers with very few green fibers noted, demonstrating the predominance of type I collagen in normal cornea and these fibers were also arranged in a precise, parallel manner (Figure 5A). Alkali burned-corneas demonstrated an increased amount of green fibers, indicating an upregulation of type III collagen compared to negative controls. The collagen fibers in the alkali-burned corneas were notably disorganized (Figure 5B). The areas of type I collagen, type III collagen, and total collagen of the control dogs and study dogs were also quantified and these values are displayed in Table 6. Although grossly obvious, the marked increase in type III collagen in the alkali-burned corneas only approached significance ($p=0.071$). There was no statistical difference in area of type I collagen or total collagen between negative control and alkali-burned corneas ($p=0.25$, $p=0.25$, respectively). A significant difference was not detected between treatment groups in regards to type I collagen area ($p=0.8$), type III collagen area ($p=0.2$) or total collagen area ($p=1.0$)

### 3.6. Presence of α-SMA Indicates Cellular Transdifferentiation

To determine the cell types present in the anterior stroma, immunohistochemistry was performed, specifically antibodies against α-SMA were used to identify fibroblasts, while leukocytes were stained with antibodies against CD18. Grades for these IHC stains are provided in Table 5. Negative control corneas did not stain positively for α-SMA or CD18, while alkali-burned corneas demonstrated marked α-SMA staining and no-moderate staining for CD18 (Figure 6B). The increase in α-SMA staining in the alkali-burned corneas was significant when compared to negative control corneas ($p=0.018$). The faint staining for CD18 in the alkali-burned corneas was not significant ($p=0.143$). A significant difference

between treatment groups was not detected with regards to the degree of α-SMA or CD18 staining (p=0.4 for both IHC).

### 3.7. Transmission Electron Microscopy Reveals Disorganization of Collagen Fibrils

Ultrastructural analysis of the corneas was utilized for analysis of stromal collagen fibril arrangement (Figure 7). Marked stromal collagen fibril disorganization, characteristic of fibrosis, was detected. Mean values of these parameters measured in control and experimental corneas are shown in Table 7. No statistical difference was noted in the area of (p= 0.108), and minimum (p= 0.26) and maximum (p=0.205) distances between collagen fibrils between left eyes of study dogs and control dogs, demonstrating that there was no breed related differences in these parameters. When comparing the study dogs, regardless of treatment group to control dogs, both the minimum and maximum distances between collagen fibrils was significantly greater for the dogs that underwent the alkali burn (p=0.026, p=0.018, respectively) as demonstrated in Figure 7. When comparing the two treatment groups to each other, there was no statistical difference in the mean area of collagen fibrils (p=0.822), the mean minimum distance between collagen fibrils (p=0.445) or the maximum distance between collagen fibrils (p=0.404).

## 4. Discussion

Current *in vivo* models of corneal fibrosis possess several limitations. The corneal anatomy of the animals commonly utilized in ophthalmic research differs significantly from that of people. For example, the mouse central corneal thickness ranges from 0.089–0.123 mm, the rat is 0.16 mm, and a rabbit has a central corneal thickness of 0.36 mm. By contrast, the central corneal thickness in people has been reported as 0.54 mm. The dog's central corneal thickness of 0.5–0.66 mm is more similar to people (Vezina 2013). Using the dog as an animal model, the responses to corneal injury and to experimental therapies are likely to be more representative of the possible responses seen in people and is therefore deemed more appropriate.

In addition to thin corneas, mice and rats have corneas that are quite small in diameter compared to people (approximately 2 mm versus 11 mm respectively) (Henriksson et al. 2009, Salouti et al. 2013). Due to their small diameter it can be difficult to isolate the axial cornea when performing an alkali burn. Induced chemical injury typically extends to the limbus resulting in a depletion of corneal limbal stem-cells. In fact, the alkali burn is commonly used to induce limbal stem-cell deficiency (LSCD) in an experimental setting (Gimeno et al. 2007) to study LSCD in people, a common sequela to chemical injury (Tseng 1989, Puangsricharern and Tseng 1995, Fatima et al. 2008). As a consequence of LSCD, corneal repair mechanisms are significantly altered, resulting in persistent ulceration, neovascularization and loss of transparency (Huang and Tseng 1991, Gu and Hu 2013). Consequently, if a corneal alkali burn model is used to assess therapies for corneal fibrosis that do not involve LSCD, the assessment of the wound healing response and the efficacy of investigative therapies may be inaccurate if rats or mice are used due to the high likelihood of limbal damage in these small species.

To better address above stated concerns in currently utilized animal models of corneal disease, our group has developed a new large animal model of corneal fibrosis. In previous studies corneal fibrosis has been generated *in vivo* with photorefractive keratectomy (PRK), repeated epithelial abrasions, penetrating keratectomy, laceration and suture placement, sulfur mustard exposure and an alkali burn. Photorefractive keratectomy requires specialized equipment, specifically an excimer laser and experienced operator. Those performing the PRK must undergo extensive training to successfully create corneal fibrosis and the resulting corneal scars can be subtle (Sharma et al. 2009). Similarly, the corneal haze caused by repeated debridement of the canine cornea by Bentley group was indistinct (Bentley et al. 2001). Previous studies have demonstrated that rodents and rabbits can tolerate a small (1 mm or less) penetrating keratectomy (Stramer et al. 2003). In contrast, full thickness corneal wounds in dogs can result in significant anterior uveitis and iris prolapse (Denis 2002). Thus, this technique was inappropriate for the translational studies. Additionally, the use of a linear laceration and suture placement (Berdahl, Johnson et al. 2009) was excluded as the presence of suture in the cornea was considered a possible confounding factor to the corneal wound healing process and an additional irritant to the dogs. Exposure to sulfur mustard can generate notable corneal fibrosis (Ruff et al. 2013). However, this chemical is a select agent and is known to cause serious injuries to other organ systems and cannot be used in normal laboratory setting due to the risk to those performing the procedure (Graham and Schoneboom 2013). Thus, the alkali burn represented the ideal method to produce corneal fibrosis as it does not require specialized training or expensive equipment, safe to people handling carefully, does not require special laboratory setting, and creates a visible corneal scar.

The present study demonstrated that the corneal alkali burn was well-tolerated by dogs, as their mMS scores continued to improve throughout the study. Only one dog was excluded from the study as the right eye developed keratomalacia. Thorough diagnostic testing, including cytology and culture, did not reveal any infectious agents. Due to the acute presentation and rapid progression of keratomalacia coupled with failure to detect any pathogens, it was suspected that the cornea of this dog experienced a traumatic event. Each dog was caged with one other dog for socialization purposes, and although the dogs tolerated their cage mate throughout the study, it is possible that this particular dog's cage mate scratched or excessively licked her affected eye. The progression of the corneal wound was deemed unrelated to the initial alkali burn, and it was appropriate to exclude this dog's clinical scores from day 11 to day 14 and also all OCT, histopathological, and TEM findings from final analysis.

The alkali burn generated significant fibrotic changes in the dog cornea. The degree of fibrotic change appeared to depend on the duration of alkali burn, as the cornea haze grade, histopathology and IHC scores were lower in the sentinel dog's right eye (15 second burn) than the left (30 second burn). The sentinel dog's corneal findings consisted of a small amount of corneal haze in the right eye and bulla formation in the left, and so we determined that optimal alkali burn time in this pilot project to be 20 seconds and this duration of alkali burn was used for all remaining study dogs.

A 20 second alkali burn was able to generate marked corneal haze and resulted in abnormalities on histopathology and IHC suggestive of fibrosis. H&E sections of the affected corneas revealed that the cellularity of the superficial stroma was markedly increased. Although a minority of these stromal cells stained positively for CD18, suggesting an inflammatory lineage, it appeared that the majority of cells stained positively for α-SMA, a known hallmark of fibrosis (Buss et al. 2010, Bosiack, Giuliano et al. 2012). This staining for α-SMA was significantly increased in the alkali-burned corneas when compared to control corneas, thereby suggesting that the alkali burn induced the transdifferentiation of corneal fibroblasts to myofibroblasts. Importantly, histopathology of affected corneas in this study did not reveal changes secondary to LSCD (Shapiro et al. 1981, Dua 1998, Fatima et al. 2008). The alkali burn protocol developed in the current study reliably created axial corneal fibrosis while preserving the limbal stem-cells.

The results of special stains, specifically Masson's trichrome and picrosirius red, confirmed development of corneal fibrosis following the alkali burn. The corneal stroma contains collagen types I, III, IV, V and VI (Doane et al. 1992, Takahashi et al. 1993, Sun et al. 2011, Herwig et al. 2013). The different collagens are assembled into banded fibrils, arranged in an orthogonal manner within the corneal stroma. This precise organization of corneal fibrils, in addition to the fixed quantity of each collagen type, allows for minimal light scattering and subsequent transparency (Hassell and Birk 2010). With the disruption of this arrangement or deposition of excess collagen of any type, corneal transparency is lost, replaced by fibrosis. Masson's trichrome stain and picrosirius red stain have been utilized to detect collagen fibers in other organ systems including the heart, kidneys and live, and increased quantity of these stains signifies fibrosis (Abo-Zenah et al. 2002, Xie et al. 2002, Chen et al. 2014, Ding et al. 2015). However, unlike the cornea, these other organs do not contain significant collagen. Therefore, in the current study, the Masson's trichrome and pircoSirius red stains had to be evaluated and scored to accommodate the cornea's native collagen content. For Masson's trichrome stained corneas the increased red staining in the anterior stroma represented mesenchymal cells, either fibroblast or vascular endothelial cells (Sanyal et al. 1998). Cell type was verified with α-SMA, confirming that the predominant cell population was composed of fibroblasts. The picrosirius red stain not only demonstrated transitions in collagen type but also in collagen fibril arrangement. It has been well established that the proportion of different corneal collagen types changes significantly during the process of fibrosis, as type I collagen which predominates in normal cornea is replaced by type III collagen in a corneal scar (Karamichos et al. 2010, Janin-Manificat et al. 2012). Analysis of the picrosirius red stain in our study showed a significant increase in type III collagen in the alkali-burned corneas compared to negative controls corneas. Finally, collagen fibrils appeared extremely disorganized with the picrosirius red stain between negative control and alkali-burned corneas supportive of collagen remodeling typical of fibrosis.

The results of the EVG stain further supported the development of corneal fibrosis following the alkali burn. EVG is used to identify elastic fibers (Lee et al. 2001). Reports of elastic fibers in the mammalian cornea are sparse and conflicting (Donovan et al. 1974, Carrington et al. 1984, Kamma-Lorger et al. 2010) and to our knowledge elastic fibers have not been detected in the axial cornea of dogs. In other organ systems, which contain some elastic

fibers normally, such as the lung, the presence and proportion of elastic fibers can determine the degree of fibrosis (Enomoto et al. 2013). Consequently, the increased quantity of this stain in the anterior stroma of the alkali-burned corneas further supports fibrotic change in this novel model.

Structural analysis of the corneas with OCT complemented histopathology findings. The corneal epithelium was variably thickened, consistent with epithelial hyperplasia, and the foci of hyper-intense signal in the anterior stroma likely represented the increased cellularity noted on histopathology. OCT is routinely used in physician ophthalmology and allows for non-contact, non-invasive imaging that assists in the diagnosis and management of several corneal diseases, including ocular surface squamous neoplasia, corneal epithelial basement membrane dystrophy, keratoconus and bullous keratopathy (Chan et al. 2011, Bouheraoua et al. 2014, Thomas et al. 2014, El Sanharawi et al. 2015). People with corneal scarring associated with an irregular Bowman's membrane undergo OCT imaging prior to phototherapeutic keratectomy (PTK) to measure the depth of their corneal scars and allow for surgical planning. A corneal scar on these OCT images is defined as (1) an area of cornea that demonstrates a hyper-intense signal that corresponds with scarring noted on clinical examination and (2) an area of cornea with variable epithelial thickness by a minimum of 33% from the baseline epithelial thickness (Rush et al. 2013). In the current study, the maximum increase in corneal epithelial thickness was 75.3%. Study dogs demonstrated hyper-intense signals within the anterior stroma of the burned area. Our OCT findings, coupled with our clinical examination findings, support the conclusion that this study protocol effectively creates corneal fibrosis in dogs similar to that described in physician ophthalmology.

Transmission electron microscopy allows for ultrastructural analysis of both normal and pathologic tissue architecture. The size of and distance between collagen fibrils in normal human cornea has been reported, and these measurements appear to be dependent on the methods of fixation and embedding resin used during processing (Akhtar 2012). Documented collagen fibril diameter and interfibrillar spacing ranges from 25–35 nm and 38.0–52.5 nm, respectively (Komai 1991, Akhtar 2012, Akhtar et al. 2014). To our knowledge, the distance between collagen fibrils in the normal canine cornea has not yet been established, while the collagen fibril diameter for normal corneas of the Beagle has been previously reported as 28.3±3.49 nm (Nagayasu et al. 2008). Investigations of these parameters in normal corneas of other dogs breeds remains non-existent. Here, it was found that the average size and spacing of the collagen fibrils did not differ from that of normal Beagle stroma in the dog breeds which served as controls (Poodle, American Pit bull terrier and mixed breed dog). Although the sample population for this analysis was small, this ultrastructual analysis represents the first comparison of corneal collagen fibril organization among different breeds. Differences in other anatomical aspects of the cornea such as nerve fiber density have been detected among different dog breeds, dependent on skull type (Kafarnik et al. 2008); it may, therefore, be of interest to pursue additional studies aimed at comparing collagen fibril size and spacing among different cat and dog breeds utilizing a larger sample population. Despite the lack of published normal values for collagen fibril size and organization in dog cornea, a significant difference in the minimum and maximum interfibrillar distance was detected between normal and wounded corneas in this study. This

increase in spacing and subsequent disorganization of corneal collagen fibrils has been previously documented in other studies evaluating corneal scars in people and laboratory animals thereby indicating that the alkali burn is able to generate corneal fibrosis (Dawson et al. 2005, McCally et al. 2007, Akhtar et al. 2014). As previously mentioned, the use of TEM is sparse in studies evaluating dog corneas, regardless of pathology. We quantified corneal fibril changes noted on TEM using advanced computer modeling via a multi-scale Hessian matrix system. This current study represents pioneering research, demonstrating the value of computer analysis of TEM images as an objective, yet highly specific means by which corneal fibrosis in dogs can be quantified in the research setting.

Interestingly, there did not appear to be difference in the degree of fibrosis between the treatment groups. Our laboratory has previously established that SAHA prevents corneal fibrosis. Specifically, Bosiak *et al*. and Donnelly *et. al*. demonstrated that SAHA prevents TGF-β1 mediated canine and equine corneal fibrosis *in vitro* and Tandon *et. al.* found that SAHA reduced corneal haze in rabbits *in vivo* following PRK (Bosiack et al. 2012, Tandon et al. 2012, Donnelly et al. 2014). While the efficacy of SAHA as an anti-fibrotic has been repeatedly demonstrated, the precise molecular mechanisms by which it inhibits fibrosis in the cornea have not been extensively investigated so far. Consequently our laboratory has sought to determine the mechanisms of action of SAHA as a corneal anti-fibrotic agent. Recent research by our laboratory has shown that SAHA inhibits corneal fibrosis by modulating both canonical (Smad) and non-canonical (ERK1/2) components of TGF-β1 intracellular signaling pathways and also matrix metalloproteinase 2 and 9 activity (Gronkiewicz unpublished data). In another recent study, which did not specifically evaluate the anti-fibrotic effects of SAHA, the various molecular mechanisms by which SAHA inhibits corneal neovascularization were determined. Here, SAHA prevented corneal neovascularization by attenuating hemangiogenesis, inflammatory pathways and lymphangiogenesis (Li et al. 2013).

Failure to detect a statistically significant difference between treatment groups may be due to the relatively small number of dogs examined in this study., The minimal number of animals deemed necessary to detect a difference between treatment and control dogs was utilized in accordance to institutional animal care and use guidelines. Six dogs were deemed appropriate after careful review of other studies that included sample sizes of 6 or less animals (Dupre and Coudek 2013, Gray et al. 2013, Naughton et al. 2013). Despite support from the literature, our small sample size increased the probability of type II error. With type II error, the null hypothesis of the study is accepted, when in fact it is false. Thus, there may have been a significant difference in the severity of fibrosis between the treatment groups. Another possible reason that the two treatment groups did not differ was the potential ineffective dosage of SAHA used in the current study. Previous studies performed by our laboratory determined that SAHA at a concentration of 25 μM was able to reduce corneal haze following PRK in rabbits *in vivo* (Tandon et al. 2012). However, that particular study design differed significantly in terms of the laboratory animal utilized and the methodology utilized to create corneal fibrosis. The alkali burn in the canine cornea creates more significant inflammation and fibrosis than PRK in the rabbit cornea. Therefore, it is possible that the concentration of SAHA needed to prevent fibrosis secondary a corneal alkali burn is

greater than 50 μM. Additional studies with larger sample size and different doses are warranted to better investigate the efficacy of SAHA as an anti-fibrotic *in vivo*.

## 5. Conclusion

The canine corneal alkali burn described here is well tolerated and does not damage the corneal limbus. The development of fibrosis was confirmed by histopathology, IHC, OCT and TEM. Treatment with SAHA did not appear to reduce severity of fibrosis in this pilot study.

## Acknowledgments

**Grant Information:** The University of Missouri Ruth M. Kraeuchi Missouri Endowed Chair Ophthalmology Fund (RRM) and the American College of Veterinary Ophthalmologists' Vision for Animals (KMG) primarily and from the National Eye Institute NIH RO1EY017294 (RRM) and Veteran Health Affairs Merit 1I01BX000357 (RRM) grants partially.

The work was primarily supported from the University of Missouri Ruth M Kraeuchi Missouri Endowment of Ophthalmology fund (RRM) and partially grants from the NEI/NIH RO1EY017294 (RRM), Veteran Health Affairs Merit 1I01BX000357 (RRM) and the American College of Veterinary Ophthalmologist's Vision for Animals grant (KMG). The authors gratefully acknowledge the technical support of Ms. Melanie Kunkel, Ms. Jessica Kitchell, and Mr. Justin L. Brooke. The authors also thank Dr. Richard W. Madsen (RWM) for performing statistical analysis.

## References

Abo-Zenah H, Katsoudas S, Wild G, De Takats D, Shortland J, Brown CB, El Nahas AM. Early human renal allograft fibrosis: Cellular mediators. Nephron. 2002; 91:112–119. [PubMed: 12021527]

Akhtar S. Effect of processing methods for transmission electron microscopy on corneal collagen fibrils diameter and spacing. Microsc Res and Tech. 2012; 75:1420–1424. [PubMed: 22648981]

Akhtar S, Alkatan H, Kirat O, Almubrad T. Ultrastructural and three-dimensional study of post-LASIK ectasia cornea. Microsc Res and Tech. 2014; 77:91–98. [PubMed: 24222271]

Bentley E, Abrams GA, Covitz D, Cook CS, Fischer CA, Hacker D, Stuhr CM, Reid TW, Murphy CJ. Morphology and immunohistochemistry of spontaneous chronic corneal epithelial defects (SCCED) in dogs. Investig Ophthalmol Vis Sci. 2001; 42:2262–2269. [PubMed: 11527939]

Berdahl JP, Johnson CS, Proia AD, Grinstaff MW, Kim T. Comparison of sutures and dendritic polymer adhesives for corneal laceration repair in an in vivo chicken model. Arch Ophthalmol. 2009; 127:442–447. [PubMed: 19365021]

Bosiack AP, Giuliano EA, Gupta R, Mohan RR. Efficacy and safety of suberoylanilide hydroxamic acid (Vorinostat) in the treatment of canine corneal fibrosis. Vet Ophthalmol. 2012; 15:307–314. [PubMed: 22212187]

Bouheraoua N, Jouve L, El Sanharawi M, Sandali O, Temstet C, Loriaut P, Basli E, Borderie V, Laroche L. Optical coherence tomography and confocal microscopy following three different protocols of corneal collagen-crosslinking in keratoconus. Investig Ophthalmol Vis Sci. 2014; 55:7601–7609. [PubMed: 25352122]

Buss DG, Giuliano EA, Sharma A, Mohan RR. Isolation and cultivation of equine corneal keratocytes, fibroblasts and myofibroblasts. Vet Ophthalmol. 2010; 13:37–42. [PubMed: 20149174]

Carrington SD, Alexander RA, Grierson I. Elastic and related fibres in the normal cornea and limbus of the domestic cat. J Anat. 1984; 139:319–332. [PubMed: 6490521]

Chan JB, Yuen LH, Huang EH, Htoon HM, He M, Aung T, Tan DT, Mehta JS. Reproducibility of cornea measurements in anterior segment OCT images of normal eyes and eyes with bullous keratopathy analyzed with the Zhongshan Assessment Program. Investig Ophthalmol Vis Sci. 2011; 52:8884–8890. [PubMed: 21828152]

Chen S, Puthanveetil P, Feng B, Matkovich SJ, Dorn GW, Chakrabarti S. Cardiac miR-133a overexpression prevents early cardiac fibrosis in diabetes. J Cell and Mol Med. 2014; 18:415–421. [PubMed: 24428157]

Dawson DG, Kramer TR, Grossniklaus HE, Waring GO 3rd, Edelhauser HF. Histologic, ultrastructural, and immunofluorescent evaluation of human laser-assisted in situ keratomileusis corneal wounds. Arch Ophthalmol. 2005; 123:741–756. [PubMed: 15955975]

Denis HM. Anterior lens capsule disruption and suspected malignant glaucoma in a dog. Vet Ophthalmol. 2002; 5:79–83. [PubMed: 12071863]

Ding H, Ma JJ, Wang WP, Zeng WJ, Jiang T, Huang BJ, Chen SY. Assessment of liver fibrosis: The relationship between point shear wave elastography and quantitative histological analysis. J Gastroenterol and Hepatol (Australia). 2015; 30:553–558.

Doane KJ, Yang G, Birk DE. Corneal cell-matrix interactions: Type VI Collagen promotes adhesion and spreading of corneal fibroblasts. Exp Cell Res. 1992; 200:490–499. [PubMed: 1572410]

Donnelly KS, Giuliano EA, Sharma A, Mohan RR. Suberoylanilide hydroxamic acid (vorinostat): its role on equine corneal fibrosis and matrix metalloproteinase activity. Vet Ophthalmol. 2014; 17:61–68. [PubMed: 25126665]

Donovan RH, Carpenter RL, Schepens CL, Tolentino FI. Histology of the normal collie eye: I Topography, cornea, sclera and filtration angle. Ann Ophthalmol. 1974; 6:257–260. passim. [PubMed: 4815893]

Dua HS. The conjunctiva in corneal epithelial wound healing. Br J Ophthalmol. 1998; 82:1407–1411. [PubMed: 9930272]

Dupre G, Coudek K. Laparoscopic-assisted placement of a peritoneal dialysis catheter with partial omentectomy and omentopexy in dogs: an experimental study. Vet Surg. 2013; 42:579–585. [PubMed: 23373768]

El Sanharawi M, Sandali O, Basli E, Bouheraoua N, Ameline B, Goemaere I, Georgeon C, Hamiche T, Borderie V, Laroche L. Fourier-Domain Optical Coherence Tomography Imaging in Corneal Epithelial Basement Membrane Dystrophy: A Structural Analysis. Am J Ophthalmol. 2015; 159:755–763. [PubMed: 25579644]

Enomoto N, Suda T, Kono M, Kaida Y, Hashimoto D, Fujisawa T, Inui N, Nakamura Y, Imokawa S, Funai K, Chida K. Amount of elastic fibers predicts prognosis of idiopathic pulmonary fibrosis. Respir Med. 2013; 107:1608–1616. [PubMed: 23993151]

Ersoy, I.; Bunyak, F.; Higgins, JM.; Palaniappan, K. Coupled edge profile active contours for red blood cell flow analysis. Biomedical Imaging (ISBI). 2012 9th IEEE International Symposium on Biomedical Imaging From Nano to Macro; 2012.

Fatima A, Iftekhar G, Sangwan VS, Vemuganti GK. Ocular surface changes in limbal stem cell deficiency caused by chemical injury: A histologic study of excised pannus from recipients of cultured corneal epithelium. Eye. 2008; 22:1161–1167. [PubMed: 17558385]

Fini ME, Stramer BM. How the cornea heals: cornea-specific repair mechanisms affecting surgical outcomes. Cornea. 2005; 24:S2–s11. [PubMed: 16227819]

Gimeno FL, Lavigne V, Gatto S, Croxatto JO, Correa L, Gallo JE. Advances in corneal stem-cell transplantation in rabbits with severe ocular alkali burns. J Cataract and Refract Surg. 2007; 33:1958–1965. [PubMed: 17964405]

Graham JS, Schoneboom BA. Historical perspective on effects and treatment of sulfur mustard injuries. Chem Biol Interact. 2013; 206:512–522. [PubMed: 23816402]

Gray LL, Hillier A, Cole LK, Rajala-Schultz PJ. The effect of ketoconazole on whole blood and skin ciclosporin concentrations in dogs. Vet Dermatol. 2013; 24:118–125. e127–118. [PubMed: 23331687]

Gray ME, West CE. Corneal injuries from liquid detergent pods. J aapos. 2014; 18:494–495. [PubMed: 25280925]

Gu HW, Hu N. Study on the establishment of corneal alkali chemical injury on rats. Int Eye Sci. 2013; 13:1093–1095.

Gu Y, Li X, He T, Jiang Z, Hao P, Tang X. The Antifibrosis Effects of Peroxisome Proliferator-Activated Receptor delta on Rat Corneal Wound Healing after Excimer Laser Keratectomy. PPAR Res. 2014; 2014:464935. [PubMed: 25477952]

Guell JL, Verdaguer P, Elies D, Gris O, Manero F. Persistent stromal scar after PRK and CXL: different preoperative findings, similar complication. J Refract Surg. 2015; 31:211–212. [PubMed: 25870865]

Guo W, Shan B, Klingsberg RC, Qin X, Lasky JA. Abrogation of TGF-beta1-induced fibroblast-myofibroblast differentiation by histone deacetylase inhibition. Am J Physiol Lung Cell Mol Physiol. 2009; 297:L864–870. [PubMed: 19700647]

Hassell JR, Birk DE. The molecular basis of corneal transparency. Exp Eye Res. 2010; 91:326–335. [PubMed: 20599432]

Henriksson JT, McDermott AM, Bergmanson JPG. Dimensions and Morphology of the Cornea in Three Strains of Mice. Investigat Ophthalmol Vis Sci. 2009; 50:3648–3654.

Herwig MC, Müller AM, Holz FG, Loeffler KU. Immunolocalization of different collagens in the cornea of human fetal eyes: A developmental approach. Curr Eye Res. 2013; 38:60–69. [PubMed: 23130612]

Huang AJ, Tseng SC. Corneal epithelial wound healing in the absence of limbal epithelium. Investigat Ophthalmol Vis Sci. 1991; 32:96–105.

Janin-Manificat H, Rovere MR, Galiacy SD, Malecaze F, Hulmes DJ, Moali C, Damour O. Development of ex vivo organ culture models to mimic human corneal scarring. Mol Vis. 2012; 18:2896–2908. [PubMed: 23233791]

Junqueira LC, Cossermelli W, Brentani R. Differential staining of collagens type I, II and III by Sirius Red and polarization microscopy. Arch Histol Jpn. 1978; 41:267–274. [PubMed: 82432]

Kadar T, Amir A, Cohen L, Cohen M, Sahar R, Gutman H, Horwitz V, Dachir S. Anti-VEGF Therapy (Bevacizumab) for Sulfur Mustard-Induced Corneal Neovascularization Associated with Delayed Limbal Stem Cell Deficiency in Rabbits. Curr Eye Res. 2013; 39:439–450. [PubMed: 24215293]

Kafarnik C, Fritsche J, Reese S. Corneal innervation in mesocephalic and brachycephalic dogs and cats: assessment using in vivo confocal microscopy. Vet Ophthalmol. 2008; 11:363–367. [PubMed: 19046276]

Kamma-Lorger CS, Boote C, Hayes S, Moger J, Burghammer M, Knupp C, Quantock AJ, Sorensen T, Di Cola E, White N, Young RD, Meek KM. Collagen and mature elastic fibre organisation as a function of depth in the human cornea and limbus. J Struct Biol. 2010; 169:424–430. [PubMed: 19914381]

Karamichos D, Guo XQ, Hutcheon AE, Zieske JD. Human corneal fibrosis: an in vitro model. Investigat Ophthalmol Vis Sci. 2010; 51:1382–1388.

Kern TJ. Ulcerative keratitis. Vet Clin North Am Small Anim Pract. 1990; 20:643–666. [PubMed: 2194352]

Komai Y, Ushiki T. The three-dimensional organization of collagen fibrils in the human cornea and sclera. Investigat Ophthalmol Vis Sci. 1991; 32:2244–2258.

Labelle AL, Psutka K, Collins SP, Hamor RE. Use of hydropulsion for the treatment of superficial corneal foreign bodies: 15 cases (1999–2013). J Am Vet Med Assoc. 2014; 244:476–479. [PubMed: 24479463]

Lee YC, Wang IJ, Hu FR, Kao WW. Immunohistochemical study of subepithelial haze after phototherapeutic keratectomy. J Refract Surg. 2001; 17:334–341. [PubMed: 11383765]

Li X, Zhou Q, Hanus J, Anderson C, Zhang H, Dellinger M, Brekken R, Wang S. Inhibition of multiple pathogenic pathways by histone deacetylase inhibitor SAHA in a corneal alkali-burn injury model. Mol Pharm. 2013; 10:307–318. [PubMed: 23186311]

McCally RL, Freund DE, Zorn A, Bonney-Ray J, Grebe R, de la Cruz Z, Green WR. Light-scattering and ultrastructure of healed penetrating corneal wounds. Investigat Ophthalmol Vis Sci. 2007; 48:157–165.

Milani BY, Milani FY, Park DW, Namavari A, Shah J, Amirjamshidi H, Ying H, Djalilian AR. Rapamycin inhibits the production of myofibroblasts and reduces corneal scarring after photorefractive keratectomy. Investigat Ophthalmol Vis Sci. 2013; 54:7424–7430.

Nagayasu A, Hosaka Y, Yamasaki A, Tsuzuki K, Ueda H, Honda T, Takehana K. A preliminary study of direct application of atelocollagen into a wound lesion in the dog cornea. Curr Eye Res. 2008; 33:727–735. [PubMed: 18798076]

Nath S, Palaniappan K, Bunyak F. Cell Segmentation Using Coupled Level Sets and Graph-Vertex Coloring. Medical Image Computing and Computer-Assisted Intervention – MICCAI 2006. Springer Berlin Heidelberg. 2006; 4190:101–108.

Naughton JF, Stewart MC, Ciobanu L, Constable PD. Contrast magnetic resonance imaging for measurement of cartilage glycosaminoglycan content in dogs: a pilot study. Vet Comp Orthop Traumatol. 2013; 26:100–104. [PubMed: 23172016]

Nelson EF, Huang CW, Ewel JM, Chang AA, Yuan C. Halofuginone down-regulates Smad3 expression and inhibits the TGFbeta-induced expression of fibrotic markers in human corneal fibroblasts. Mol Vis. 2012; 18:479–487. [PubMed: 22393274]

Okada Y, Shirai K, Reinach PS, Kitano-Izutani A, Miyajima M, Flanders KC, Jester JV, Tominaga M, Saika S. TRPA1 is required for TGF-beta signaling and its loss blocks inflammatory fibrosis in mouse corneal stroma. Lab Invest. 2014; 94:1030–1041. [PubMed: 25068659]

Pan H, Chen J, Xu J, Chen M, Ma R. Antifibrotic effect by activation of peroxisome proliferator-activated receptor-gamma in corneal fibroblasts. Mol Vis. 2009; 15:2279–2286. [PubMed: 19936025]

Pascolini D, Mariotti SP. Global estimates of visual impairment: 2010. Br J Ophthalmol. 2012; 96:614–618. [PubMed: 22133988]

Puangsricharern V, Tseng SCG. Cytologic evidence of corneal diseases with limbal stem cell deficiency. Ophthalmology. 1995; 102:1476–1485. [PubMed: 9097795]

Pumphrey SA, Pizzirani S, Pirie CG. 360-degree conjunctival grafting for management of diffuse keratomalacia in a dog. Vet Ophthalmol. 2011; 14:209–213. [PubMed: 21521447]

Robaei D, Watson S. Corneal blindness: a global problem. Clin Exp Ophthalmol. 2014; 42:213–214.

Ruff AL, Jarecke AJ, Hilber DJ, Rothwell CC, Beach SL, Dillman JF 3rd. Development of a mouse model for sulfur mustard-induced ocular injury and long-term clinical analysis of injury progression. Cutan Ocul Toxicol. 2013; 32:140–149. [PubMed: 23106216]

Rush SW, Han DY, Rush RB. Optical coherence tomography-guided transepithelial phototherapeutic keratectomy for the treatment of anterior corneal scarring. Am J Ophthalmol. 2013; 156:1088–1094. [PubMed: 24075433]

Salouti R, Nowroozzadeh MH, Zamani M, Ghoreyshi M, Khodaman AR. Comparison of Horizontal corneal diameter measurements using the Orbscan IIz and Pentacam HR systems. Cornea. 2013; 32:1460–1464. [PubMed: 24055904]

Sanyal AJ, Contos MJ, Yager D, Zhu Y-n, Willey A, Graham MF. Development of pseudointima and stenosis after transjugular intrahepatic portasystemic shunts: Characterization of cell phenotype and function. Hepatol. 1998; 28:22–32.

Sato T. A modified method for lead staining of thin sections. J Elect Microsc. 1968; 17:158–159.

Shapiro MS, Friend J, Thoft RA. Corneal re-epithelialization from the conjunctiva. Investigat Ophthalmol Vis Sci. 1981; 21:135–142.

Sharma A, Mehan MM, Sinha S, Cowden JW, Mohan RR. Trichostatin a inhibits corneal haze in vitro and in vivo. Investigat Ophthalmol Vis Sci. 2009; 50:2695–2701.

Sharma A, Sinha NR, Siddiqui S, Mohan RR. Role of 5′TG3′-interacting factors (TGIFs) in Vorinostat (HDAC inhibitor)-mediated corneal fibrosis inhibition. Mol Vis. 2015; 28:974–984. [PubMed: 26330748]

Soille, P. Morphological Image Analysis: Principles and Applications. Springer-Verlag Telos; 1999. p. 170-171.

Stramer BM, Zieske JD, Jung JC, Austin JS, Fini ME. Molecular mechanisms controlling the fibrotic repair phenotype in cornea: implications for surgical outcomes. Investigat Ophthalmol Vis Sci. 2003; 44:4237–4246.

Sun M, Chen S, Adams SM, Florer JB, Liu H, Kao WWY, Wenstrup RJ, Birk RJ. Collagen V is a dominant regulator of collagen fibrillogenesis: Dysfunctional regulation of structure and function in a corneal-stroma-specific Col5a1-null mouse model. J Cell Sci. 2011; 124:4096–4105. [PubMed: 22159420]

Sun M, Huang J, Bunyak F, Gumpper K, De G, Sermersheim M, Liu G, Lin PH, Palaniappan K, Ma J. Superresolution microscope image reconstruction by spatiotemporal object decomposition and

association: application in resolving t-tubule structure in skeletal muscle. Opt Express. 2014; 22:12160–12176. [PubMed: 24921337]

Takahashi T, Cho HI, Kublin CL, Cintron C. Keratan sulfate and dermatan sulfate proteoglycans associate with type VI collagen in fetal rabbit cornea. J Histochem Cytochem. 1993; 41:1447–1457. [PubMed: 8245404]

Tandon A, Tovey JC, Waggoner MR, Sharma A, Cowden JW, Gibson DJ, Liu Y, Schultz GS, Mohan RR. Vorinostat: a potent agent to prevent and treat laser-induced corneal haze. J Refract Surg. 2012; 28:285–290. [PubMed: 22386369]

Thomas BJ, Galor A, Nanji AA, El Sayyad F, Wang J, Dubovy SR, Joag MG, Karp CL. Ultra high-resolution anterior segment optical coherence tomography in the diagnosis and management of ocular surface squamous neoplasia. Ocul Surf. 2014; 12:46–58. [PubMed: 24439046]

Tseng SCG. Concept and application of limbal stem cells. Eye. 1989; 3:141–157. [PubMed: 2695347]

Vezina, M. Comparative Ocular Anatomy in Commonly Used Laboratory Animals. In: Weir, AaCM., editor. Assessing Ocular Toxicology in Laboratory Animals. Springer; 2013. p. 23-52.

Vincent L, Soille P. Watersheds in digital spaces: an efficient algorithm based on immersion simulations. Pattern Analysis and Machine Intelligence, IEEE Transactions on Pattern Analysis and Machine Intelligence. 1991; 13:583–598.

Whittaker, LRaP. Collagen and picrosirius red staining: a polarized light assessment of fibrillar hue and spatial distribution. Braz J Morphol Sci. 2005; 22:97–104.

Xie SB, Yao JL, Zheng SS, Yao CL, Zheng RQ. The levels of serum fibrosis marks and morphometric quantitative measurement of hepatic fibrosis. Hepatobiliary and Pancreatic Diseases International. 2002; 1:202–206. [PubMed: 14607739]

Zhou Q, Yang L, Wang Y, Qu M, Chen P, Wang Y, Xie L, Zhao J, Wang Y. TGFbeta mediated transition of corneal fibroblasts from a proinflammatory state to a profibrotic state through modulation of histone acetylation. J Cell Physiol. 2010; 224:135–143. [PubMed: 20232294]

## Highlights

- The anatomy and physiology of the dog cornea is similar to human.
- The alkali burn protocol successfully created corneal fibrosis in dogs.
- A novel in vivo model of corneal fibrosis was developed in dogs.
- This model is useful for evaluating safety and efficacy of newer therapeutics in large animals.
- SAHA is safe for topical eye application to treat corneal fibrosis *in vivo*.

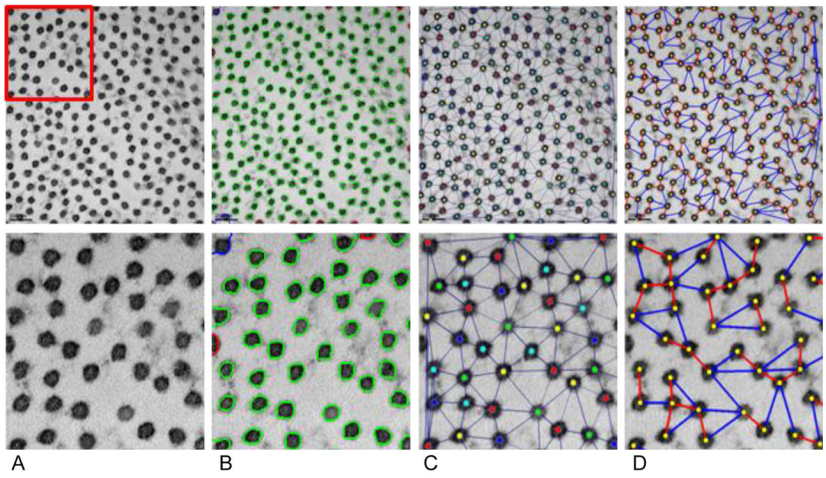


**Figure 1.**

Image analysis and quantification for TEM images of collagen fibril cross-sections. First row: original image at 25,000X magnification; second row: magnified region. A) Original TEM image. B) Collagen fibril segmentation results. D) Fibril centroids and fibril neighborhood graph. D) Nearest (red) and farthest (blue) immediate neighbors.

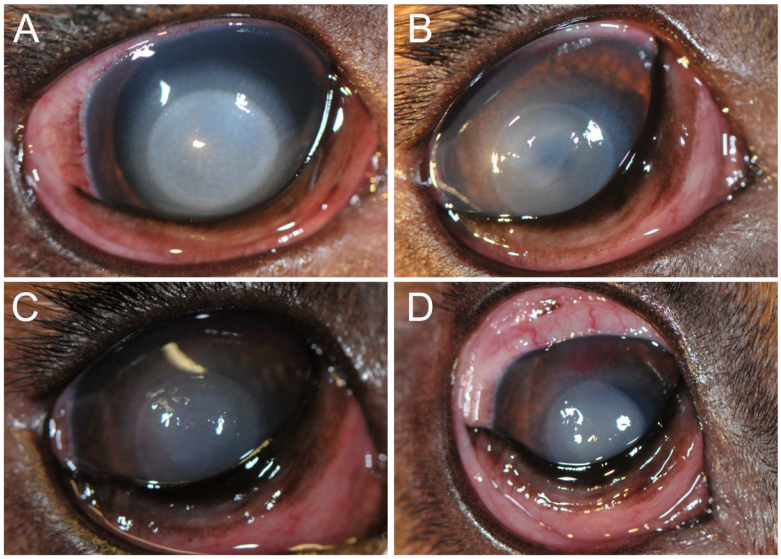


**Figure 2.**

Clinical scores and corneal haze grades following the 20 second alkali burn in a representative dog. A) One day following alkali burn, the mMS score was 17.5 and corneal haze grade was 3. B) On day 5 the mMS score was 11 and corneal haze grade was 2. C) Ten days post-alkali burn the mMS score was 8.5 and corneal haze grade was 2. D) At the study's endpoint (day 14), the mMS score was 6.5 and corneal haze grade was 2.

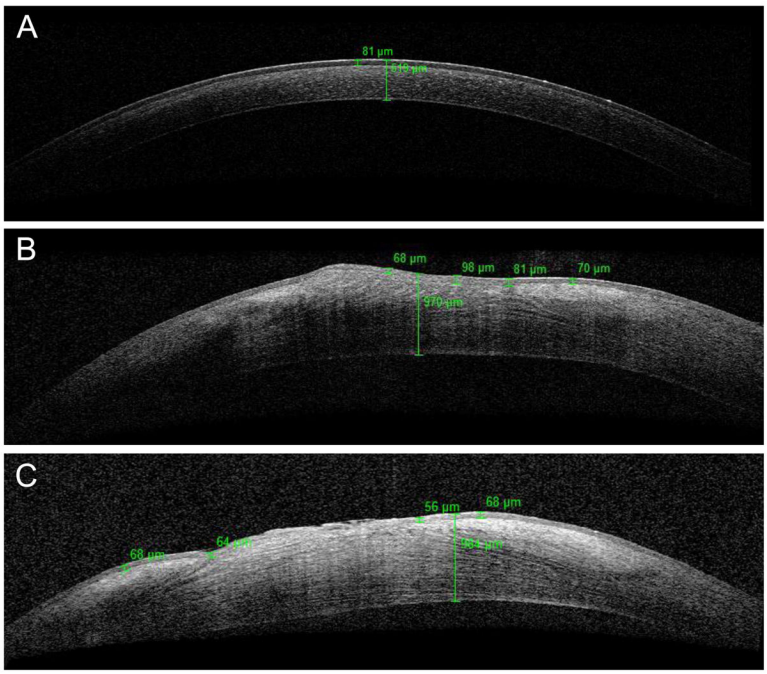


**Figure 3.**

Representative OCT images of normal cornea at baseline and alkali-burned cornea 14 days after wounding. A) Normal cornea of a dog prior to wounding. The values in green represent epithelial and total corneal thickness. B) Alkali-burned cornea from dog in treatment group A. C) Alkali-burned cornea from dog in treatment group B. Note the variable epithelial thickness and the increased total corneal thickness in the alkali-burned cornea compared to the normal cornea at baseline.

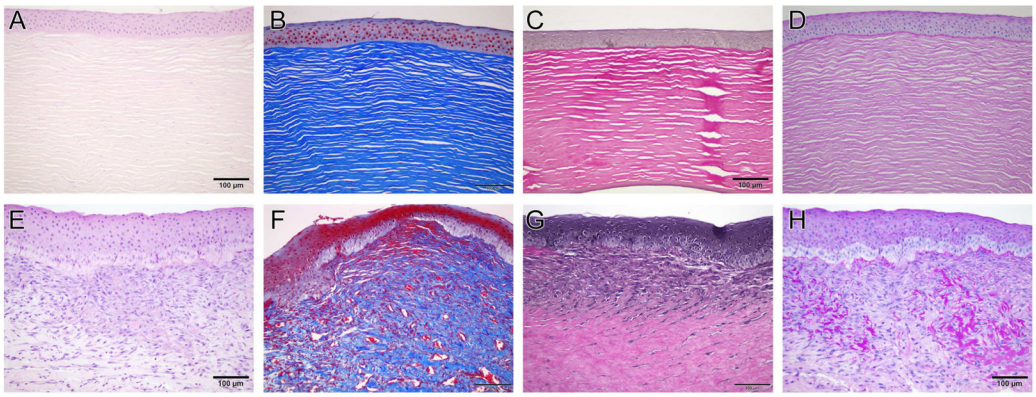


**Figure 4.**

Representative histological images of normal (A–D) and alkali-burned corneas (E–H). H&E stain demonstrated an increased cellularity of the anterior stroma in the alkali-burned corneas (E) compared to normal corneas (A). Masson's trichrome stain of the alkali-burned cornea (F) confirmed presence of mesenchymal cells in the anterior stroma, which are absent in normal cornea (B). The formation of elastic fibers was demonstrated in the alkali-burned cornea with EVG (G). No elastic fibers were detected in normal cornea (C). PAS stained corneas showed increased basement membrane and fibrin deposition in the alkali-burned cornea (H) compared to normal cornea (D).

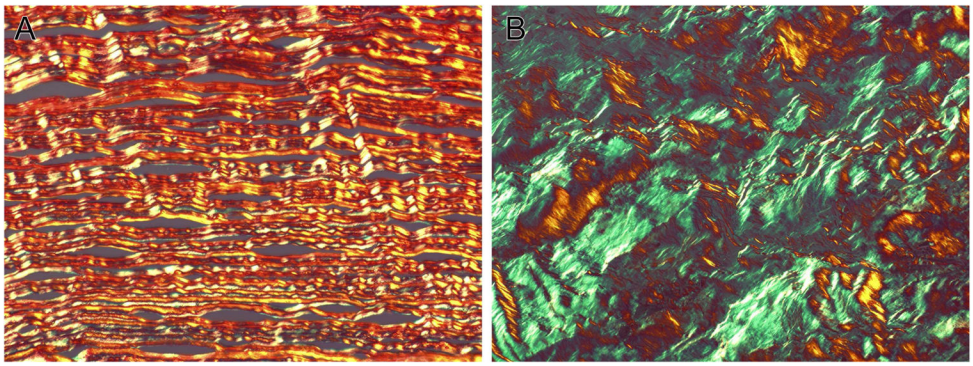


**Figure 5.**

Representative Picrosirius red stained negative control (A) and alkali-burned (B) corneas. Note the increased amount of type III collagen fibers in the alkali-burned cornea compared to the negative control. This transition of type I to type III collagen fibers is typical of scar formation.

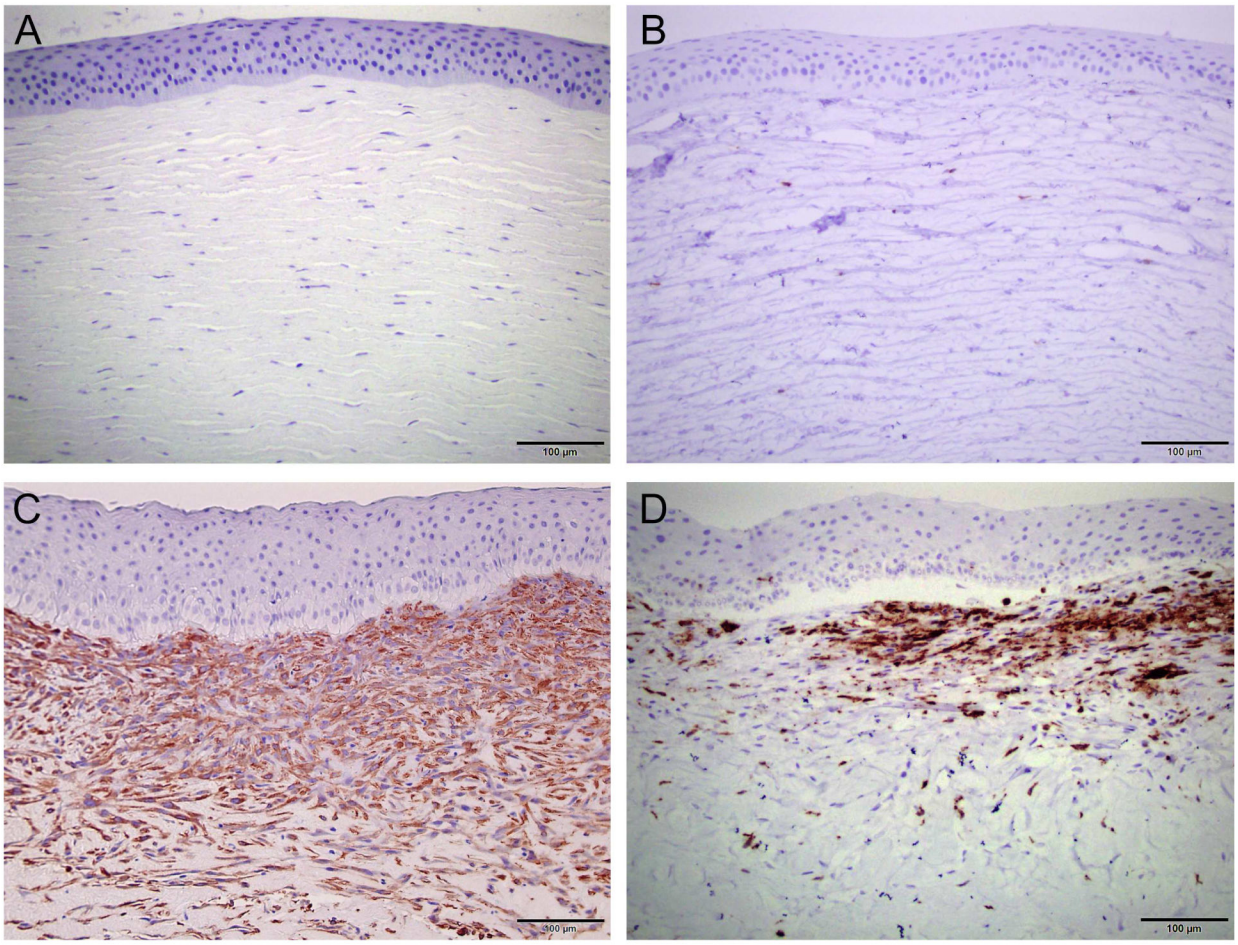


**Figure 6.**

Representative immunohistochemistry of normal (A) and alkali-burned (B) corneas. Increased α-smooth muscle actin stain in the alkali-burned corneas confirmed the cell population in the anterior stroma as fibroblasts. There was only a mild-moderate increase in CD18 stain in the alkali-burned cornea indicating that the majority of the cellular infiltrate was not inflammatory in nature.

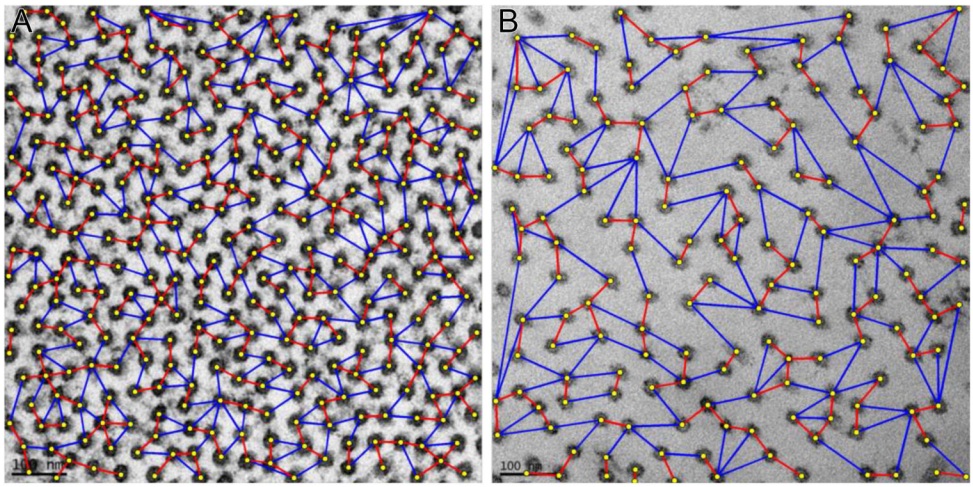


**Figure 7.**

Representative transmission electron microscopy images of normal cornea (A) and alkali-burned (B) corneas, specifically measuring the minimum and maximum interfibrillar distances. Note the increased minimum (red) and maximum (blue) interfibrillar distances in the alkali-burned cornea compared to normal cornea.

**Table 1**

Tissue targets of special histopathology stains

| Stain | Target | Result Scored |
|---|---|---|
| Masson's Trichrome | Mesenchymal cells | Red stain |
| Elastica van Gieson | Elastic fibers | Black stain |
| Periodic acid-Schiff | Basement membrane and fibrin | Dark pink-light purple |

**Table 2**

Scoring system for severity of corneal neovascularization, edema and stain

| Score | Severity of neovascularization, edema or staining |
|---|---|
| 0 | No neovascularization, edema or staining noted |
| 1 | Mild neovascularization, edema or staining |
| 2 | Moderate neovascularization, edema or staining |
| 3 | Marked neovascularization, edema or staining noted |

**Table 3**

Possible orientation patterns based on the value of eigenvalues $\lambda_1$, $\lambda_2$ of the Hessian matrix ($|\lambda_1| \geq |\lambda_2|$) [Frangi1998].

| $\lambda_1$ | $\lambda_2$ | **Orientation Pattern** |
|---|---|---|
| Low | Low | Flat or Noise no preferred direction |
| High − | Low | Bright tubular structure |
| High + | Low | Dark tubular structure |
| High − | High − | Bright blob-like structure |
| High + | High + | Dark blob-like structure |

**Table 4**

Epithelial and total corneal thickness measurements at baseline and following the alkali burn. Multiple measurements of epithelium performed after alkali burn are expressed as a mean.

| Dog | Baseline Epithelial Thickness (μm) | Baseline Total Corneal Thickness (μm) | Post Burn Epithelial Thickness (μm) | Post Burn Total Corneal Thickness (um) |
|---|---|---|---|---|
| Sentinel Dog OD | 80 | 600 | 116.75 | 499 |
| Sentinel Dog OS | 80 | 576 | 114.25 | 973 |
| Dog 1 (Treatment A) | 79 | 498 | 101.5 | 643 |
| Dog 2 (Treatment A) | 76 | 582 | 72 | 944 |
| Dog 4 (Treatment B) | 78 | 530 | 60.25 | 986 |
| Dog 5 (Treatment B) | 73 | 506 | 107.5 | 981 |
| Dog 6 (Treatment B) | 81 | 519 | 107.5 | 980 |

**Table 5**

Scores for severity of corneal neovascularization, corneal edema and special stains

| Dog | CNV | Corneal Edema | MT | EVG | PAS | α-SMA | CD18 |
|---|---|---|---|---|---|---|---|
| Representative control dog | 0 | 0 | 0 | 0 | 0 | 0 | 0 |
| Dog 1 (Treatment A) | 0 | 0 | 0 | 0 | 0 | 2 | 0 |
| Dog 2 (Treatment A) | 2 | 1 | 2 | 3 | 2 | 3 | 2 |
| Dog 4 (Treatment B) | 2 | 3 | 2 | 3 | 2 | 3 | 2 |
| Dog 5 (Treatment B) | 3 | 1 | 3 | 3 | 1 | 3 | 2 |
| Dog 6 (Treatment B) | 3 | 3 | 2 | 3 | 3 | 3 | 2 |

## Table 6

Area of type I collagen, type III collagen and total collagen in the wound bed (alkali-burned corneas) and axial cornea (control cornea)

| Dog | Area of Type I Collagen ($\mu m^2$) | Area of Type III Collagen ($\mu m^2$) | Area of Total Collagen ($\mu m^2$) |
|---|---|---|---|
| Control dog | 35887 | 1136 | 37023 |
| Control dog | 38446 | 385 | 38831 |
| Control dog | 39563 | 618 | 40181 |
| Dog 1 (Treatment A) | 41526 | 1539 | 43065 |
| Dog 2 (Treatment A) | 5083 | 763 | 5846 |
| Dog 4 (Treatment B) | 21329 | 15531 | 36860 |
| Dog 5 (Treatment B) | 22345 | 1725 | 24070 |
| Dog 6 (Treatment B) | 4673 | 5382 | 10055 |

**Table 7**

Corneal collagen fibril dimensions measured with TEM

| Group | Collagen Fibril Area ($nm^2$) | Minimum Interfibrillar Distance (nm) | Maximum Interfibrillar Distance (nm) |
|---|---|---|---|
| Control Dogs (n= 3) | 763.428 ± 0.00005 | 42.960 ± 2.680 | 70.144 ± 5.427 |
| Beagles: Left Eye (n= 7) | 877.309 ± 168.889 | 45.377 ± 4.777 | 74.410 ± 7.9 |
| Beagles: Alkali-burned (n= 5) | 845.558 ± 113.119 | 47.829 ± 3.304 | 92.621 ± 14.774 |
| Beagles: Treatment A (n= 2) | 835.304 ± 85.467 | 46.58 ± 3.022 | 86.372 ± 3.426 |
| Beagles: Treatment B (n= 3) | 852.394 ± 131.628 | 48.66 ± 3.34 | 96.787 ± 17.951 |